pp. 1–17 (2024)

Junction conditions for one-dimensional network hemodynamic model for total cavopulmonary connection using physically informed deep learning technique

T. K. Dobroserdova[a], A. A. Isaev[a], A. A. Danilov[ab], and S. S. Simakov[*cab]

Abstract — This paper presents a novel methodology utilizing physics-informed neural network (PINN) as a junction condition for a 1D network model of blood flow in total cavopulmonary connection generated by the Fontan procedure. The technique integrates a 3D mesh generation process based on the parameterization of the junction geometry, along with a sophisticated physically regularized neural network architecture. Synthetic datasets are produced using 3D steady Stokes simulations within fixed boundaries. We use a physically informed feedforward neural network that utilizes a physically regularized loss function, which incorporates the principle of mass conservation. Our PINN achieves a tolerance of 6% on the test set. We develop a 1D-PINN multiscale model based on a previously developed method for multiscale 1D–3D simulations. Comparison with 1D–3D Stokes based model and 3D Navier–Stokes based model verifies the 1D-PINN model. In the first and second comparison, the maximum deviations of the averaged pressures and flows do not exceed 1.48% and 12.26%, respectively.

Keywords: Physics-informed neural networks, blood flow dynamics, computational hemodynamics, 3D mesh generation, physically informed neural network, Fontan circulation

MSC 2010: 65D18, 37M05, 92B20, 68U20, 68T05

Understanding blood flow dynamics in human vascular bifurcations is crucial for simulating hemodynamics in the presence of cardiovascular diseases and for developing effective treatment strategies. Accurate estimation of blood flow parameters, such as pressure and flow, in these complex regions is essential for making informed clinical decisions based on numerical simulations. The intricate interactions between various hemodynamic factors and the complexity of blood flow, particularly in situations such as the Fontan operation, present significant challenges to precise estimation.

Palliative surgery is commonly performed on patients with congenital heart disease (CHD). Typically, the initial stage of palliative surgery involves creating a systemic-pulmonary shunt at birth to prepare the lung bed for subsequent operations. The second stage is the bidirectional cavopulmonary anastomosis (BCPA), also known as the Glenn operation, in which the trunk of the lung is detached from

[a]Marchuk Institute of Numerical Mathematics of RAS, Moscow 119333
[b]Sechenov University, Moscow 119435
[c]Moscow Institute of Physics and Technology, Dolgoprudny 141701.
* E-mail: simakov.ss@phystech.edu
This work has been supported by the Russian Science Foundation, grant No. 21-71-30023.

the heart, and the superior vena cava is connected to the pulmonary artery. The final stage, known as the total cavopulmonary connection (TCPC) or the Fontan operation, is considered a highly effective method for redirecting blood from the inferior vena cava to the pulmonary arteries. However, despite surgical correction, the complication rate remains high, and the quality of life for patients is often poor. A model-based understanding of Fontan circulation and optimizing the Fontan operation can enhance prognosis for real patients [23].

3D models of blood flow enable clinicians to test various vessel configurations and flow conditions. These models help to minimize pulmonary and TCPC resistance, reduce energy dissipation in the TCPC, balance hepatic and total flow distribution between the right and left lungs, and avoid regions with excessive or low wall shear stress. Local three-dimensional blood flow modelling is frequently used to address such issues [15, 22]. The integration domain comprises the junction of the inferior and superior vena cava (IVC and SVC) and the left and right pulmonary artery (LPA and RPA). Rapid evaluation of hemodynamic parameters without solving complex Navier–Stokes equations is desirable for clinical software.

In recent years, the convergence of deep learning and computational fluid dynamics has shown significant potential in addressing the challenges mentioned above [9]. Researchers have investigated the use of Physics-Informed Neural Networks (PINNs) to bridge the gap between complex physical phenomena and data-driven predictive models. The primary benefit of PINNs is their capacity to incorporate prior knowledge of the fundamental physical laws that govern fluid flow, enabling the development of robust models capable of handling complex vascular geometries effectively.

In [3], a PINN was developed to estimate aortic hemodynamics using dimensionless Navier–Stokes equations and the divergence-free equation for additional physical regularization. In [14], cerebral hemodynamics was estimated using PINNs, with neural networks trained to satisfy conservation of mass and momentum at all junction points in the arterial tree.

This paper investigates the use of PINNs for estimating blood flow parameters in human vascular junctions following the Fontan procedure. The focus is on developing an integrated methodology that combines data generation techniques with advanced neural network architectures. After successful training, the neural network can operate without requiring substantial computational resources during application with high accuracy of a 3D model.

We describe the training process for a physically regularized neural network, starting with the creation of synthetic datasets using Latin Hypercube sampling (LHS). First, a parametric set of 3D meshes was generated using the GMSH library [4], considering the physiological ranges of radii and angles at the junction of the four vessels. Next, 3D simulations of blood flow were performed for each geometry, employing steady Stokes equations with fixed boundaries within a computational domain representing rigid vessel walls. The input parameters consist of mean pressure values at the inflow and outflow boundaries and geometric characteristics of vascular junction, while the output parameters include mean flow values

at these boundaries. Ideally, the training dataset should be derived from real patient data, necessitating extensive measurements across a wide range of parameter values — an effort that is currently challenging with existing equipment capabilities. To overcome this challenge, we generate synthetic data using a 3D steady Stokes finite element solver.

Additionally, we explore physically regularized loss function (PRLF). We propose a PRLF implementation that includes a mass conservation condition. The Adam optimization algorithm is used to minimize the loss functions [7], achieving an average relative error of 10%. The integration of PRLF with LHS facilitated convergence on a reduced dataset, resulting in a lower relative error of approximately 6% on the test dataset.

In this work, we use a previously developed PINN for estimating blood flow parameters in four-vessel junction generated by the Fontan procedure [6]. Additional data augmentation was conducted by duplicating symmetric cases in the dataset. The hyperparameters were fine-tuned using the Multi-Objective Tree-structured Parzen Estimator (MOTPE) method. PINN was trained using 3D steady Stokes equations without convective term in a 3D domain. It predicts average flows at the inputs and outputs basing on the average pressures and parameters of the 3D geometry. In this paper, we use this PINN for the first time as a boundary condition for connecting four 1D elements. This method provides better precision compared to the prevalent 0D static pressure and flow conservation assumptions, facilitating the integration of dependency on the angles of vascular junctions.

The proposed model is evaluated through a comparative analysis with simulations generated by the previously developed multiscale 1D-3D model [2] and with a 3D model. The 1D-3D model employs the steady Stokes equations, whereas our 3D model is based on the fundamental Navier–Stokes equations. As the training dataset is generated by the 3D Stokes solver, the 1D-PINN model provides similar results to the 1D-3D model with the Stokes simulation in the 3D junction domain. Although exploiting the 3D incompressible Navier–Stokes equations gives a better physical model, in our future research we shall use 3D fluid-structure interaction simulations in TCPC for training and test datasets as the most physiologically appropriate model of flows in TCPC.

The paper is organized as follows. In Section 1 we briefly describe design of PINN. In Section 2 we propose a new technique for using PINN as boundary conditions for 1D network model. In Section 3 we discuss the results of PINN training and validation of 1D-PINN network model. In Section 4 we discuss the features of the new approach and future work.

Abbreviations

In the present paper we have used the following abbreviations:
TCPC — total cavopulmonary connection;
IVC — inferior vena cava;
SVC — superior vena cava;

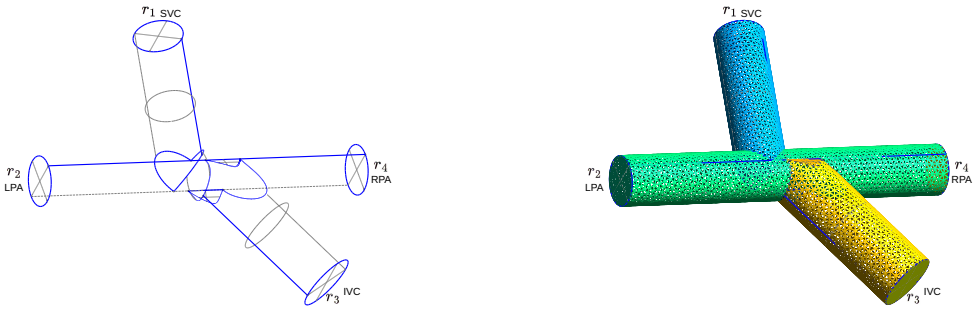

(a) Markup of the mesh surface (b) Unstructured mesh generation

Figure 1. 3D mesh generation algorithm of a four vessels junction.

RPA — right pulmonary artery;
LPA — left pulmonary artery;
PRLF — physically regularized loss function;
PINN — physically informed neural network;
LHS — latin hypercube sampling.

1. Physically informed neural network for blood flow simulation in the total cavopulmonary connection

1.1. Dataset generation

The dataset for the training and testing phases contains average pressure and flow values at the boundaries of the four-vessel junction. We compute the flows using a 3D geometry and stationary Stokes equations within a domain with fixed boundaries (see Fig. 1).

The junction geometry is parameterized by the angles α and β between the vessels, the radii r_j of each vessel and the shift in junction dx (see Fig. 2). We have developed a parametric mesh generation software using the GMSH [4] library to automate the construction of 3D meshes for a four-vessel junction. The computational domain is defined as the union of several cylindrical tubes (see Fig.1a). A quasi-uniform mesh is then constructed in this domain (see Fig. 1b). After constructing the mesh, further mesh cosmetics is applied using the Ani3D [19] package.

The blood is assumed to be a viscous incompressible fluid with viscosity $\nu = 0.04$ cm^{2}s^{-1} and density $\rho = 1$ g/cm^3. The 3D domain of junction of four vessels Ω (see Fig. 1b) with boundary $\partial\Omega$ is composed of rigid walls Γ_0, two inlets $\Gamma_{1,2}$ and two outlets $\Gamma_{3,4}$. The blood flow in Ω is described by the steady 3D Stokes equations as follows

$$\begin{aligned} -\nu\Delta\mathbf{u} + \nabla p &= \mathbf{0} \\ \operatorname{div}\mathbf{u} &= 0 \quad \text{in } \Omega \\ \mathbf{u} &= \mathbf{0} \quad \text{on } \Gamma_0 \\ \nu\frac{\partial\mathbf{u}}{\partial\mathbf{n}} - p\mathbf{n} &= p_j\mathbf{n} \quad \text{on } \Gamma_j, \;\; j = 1,\dots,4 \end{aligned} \tag{1.1}$$

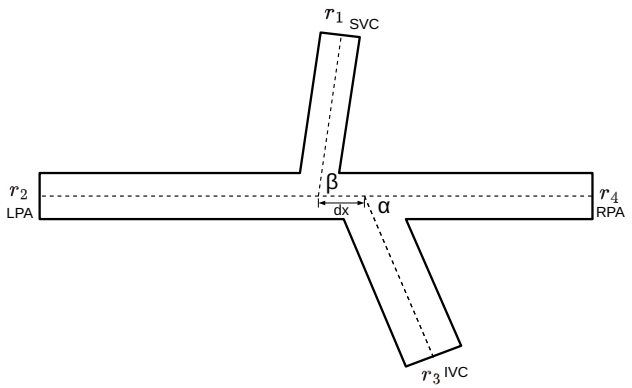

Figure 2. Parameterization of the four vessels junction: inferior vena cava (IVC), superior vena cava (SVC), left pulmonary artery (LPA), right pulmonary artery (RPA).

where p is the pressure, $\mathbf{u}$ is the velocity vector field, $\mathbf{n}$ is the outward normal vector to the boundary surface, p_j is average pressure on Γ_j. On immobile side wall, we assume no-slip and no-penetration boundary condition.

LBB-stable Taylor–Hood (P2/P1) finite element method [21] is used for the approximation of (1.1). Multifrontal sparse direct solver MUMPS [1] based on exact factorization of the matrix is applied for solving the resulted system of equations. Blood flow rates q_j on the boundaries Γ_j $(j = 1,\ldots,4)$ are calculated for further neural network training as follows

$$q_j = \int_{\Gamma_j} \mathbf{u}\cdot\mathbf{n}\,\mathrm{d}s, \quad j = 1,\ldots,4. \tag{1.2}$$

1.2. Design of the neural network

A feed-forward neural network (FFNN) establishes a mapping

$$\left\{\{p_j\}_{j=1}^4, \{r_j\}_{j=1}^4, \alpha, \beta, dx\right\} \longrightarrow \{q_j\}_{j=1}^4. \tag{1.3}$$

The specification of FFNN involves determining the number of layers and neurons, selecting an activation function for each neuron, defining a loss function based on the connection weights between neurons, implementing a dropout algorithm to randomly disconnect certain neurons from the network, and establishing an optimization procedure to minimize the loss function with respect to the weights.

Input and output layer sizes are predefined, with the first layer containing input parameters (eleven neurons) and the last one matching predicted parameters (four neurons). Determining the size of the hidden layers is challenging, and we explore two approaches for that. In this study, the dropout algorithm [18] is employed. This algorithm randomly removes neurons according to a pre-established probability. This process assists in preventing the network from overfitting to the input data, thereby enhancing its ability to generalize.

We set the activation function as

$$\mathrm{ReLU}(\varkappa) = \max(0, \varkappa) \tag{1.4}$$

where $\varkappa$ is the sum of the outputs from the previous layer neurons. Compared to other forms of activation functions, $\mathrm{ReLU}(\varkappa)$ requires less computational resources during training [8]. This allows for more efficient numerical experiments.

We set the loss (error) function as

$$\mathrm{PRLF}(\mathbf{q}, \hat{\mathbf{q}}) = \mathrm{MSE}(\mathbf{q}, \hat{\mathbf{q}}) + \mathrm{PhysLoss}(\mathbf{q}) \tag{1.5}$$

where $\mathbf{q} = \{q_1, q_2, q_3, q_4\}$ are the predicted values, and $\hat{\mathbf{q}} = \{\hat{q}_1, \hat{q}_2, \hat{q}_3, \hat{q}_4\}$ are the true values, MSE is the mean squared error

$$\mathrm{MSE}(\mathbf{q}, \hat{\mathbf{q}}) = \frac{1}{n} \sum_{i=1}^{n} \sum_{j=1}^{4} (q_{ji} - \hat{q}_{ji})^2 \tag{1.6}$$

and PhysLoss is a physical component

$$\mathrm{PhysLoss}(\mathbf{q}) = \frac{\xi}{n} \sum_{i=1}^{n} \left(\sum_{j=1}^{4} q_{ji} \right)^2 \tag{1.7}$$

where ξ is the weight coefficient, n is the number of training simulations (i.e., rows in the dataset), i is index of a training simulation, j is index of inlet or outlet boundary Γ_j of the 3D domain (see Fig. 1). We refer the neural network with PRLF as a physically informed neural network (PINN) [11], since it imposes penalties on the model for deviating from physical constraints, which in our case ensures mass conservation

$$\sum_{j=1}^{4} q_j = 0. \tag{1.8}$$

In order to assess comprehensively the performance of the PINN during the training process, we use two different error metrics, namely, Relative Error (RE) and R-squared (R2). RE provides a relative measure of the model accuracy across all data points by measuring the average percentage deviation between the true target values $\mathbf{q}$ and the predicted values $\hat{\mathbf{q}}$. R2 quantifies the fit of the model by assessing the proportion of variability in the target variables. A higher value of R2 indicates a better fit, with 1 indicating a perfect fit and 0 indicating no explanatory power.

We set RE and R2 as

$$\mathrm{RE} = \frac{1}{n} \sum_{i=1}^{n} \sum_{j=1}^{4} \frac{|q_{ji} - \hat{q}_{ji}|}{|\hat{q}_{ji}|} \tag{1.9}$$

$$\mathrm{R2} = 1 - \frac{\sum_{i=1}^{n} \sum_{j=1}^{4} (q_{ji} - \hat{q}_{ji})^2}{\sum_{i=1}^{n} \sum_{j=1}^{4} \left(q_{ji} - \overline{q}_j\right)^2} \tag{1.10}$$

where $\overline{q}$ is the mean value of the observed values

$$\overline{q}_j = \frac{1}{n}\sum_{i=1}^{n} q_{ij}. \tag{1.11}$$

By including both RE and R2, we obtain a comprehensive understanding of the accuracy of the model, which captures both relative deviation and overall explanatory power. Division by zero in (1.9) and (1.10) is not possible: $\hat{q}_{ji} \neq 0$ due to the boundary conditions in the considered model with static nature, $q_{ji} - \overline{q}_j \neq 0$ since the flows occur in assigned directions.

The training of the neural network utilizes the error backpropagation algorithm [12]. The most effective technique is currently regarded as the Adam implementation [7].

2. 1D network hemodynamic model for total cavopulmonary connection with PINN boundary conditions

In the 1D blood flow model every vessel is represented by a long axisymmetric elastic tube. Blood is considered as a viscous incompressible fluid with density ρ. In every tube 1D mass and momentum conservation laws have the form

$$\begin{gathered} \frac{\partial S}{\partial t} + \frac{\partial (S\overline{u})}{\partial x} = 0 \\ \frac{\partial \overline{u}}{\partial t} + \frac{\partial (\overline{u}^2/2 + p/\rho)}{\partial x} = 0, \quad x \in [0,l], \;\; t \in [0,T] \end{gathered} \tag{2.1}$$

and the constitutive equation has the form

$$p = \rho c_0^2 f(S) \tag{2.2}$$

where $\overline{u}$ is the linear velocity averaged over the cross-section, p is the blood pressure averaged over the cross-section, S is the area of the cross-section, c_0 is the velocity of the small disturbance propagation in the material of the vessel wall. The constitutive equation (2.2) relates the pressure to the cross-section area and describes elastic properties of the vessel wall [20]. We set this function for each vessel as

$$f(S) = \begin{cases} \exp(S\widehat{S}^{-1} - 1) - 1, & S > \widehat{S} \\ \ln(S\widehat{S}^{-1}), & S \leqslant \widehat{S} \end{cases} \tag{2.3}$$

where $\widehat{S}$ is the cross-section area of the vessel at rest. For initial conditions, the mean velocity and the cross-section area are prescribed, $\overline{u}|_{t=0} = u_0$, $S|_{t=0} = \hat{S}$.

System (2.1) is hyperbolic and can be integrated by the grid-characterstic method [10]. The boundary conditions in the vascular junction include numerical discretization along outgoing characteristic [16]:

$$\overline{u} = \psi S + \xi \tag{2.4}$$

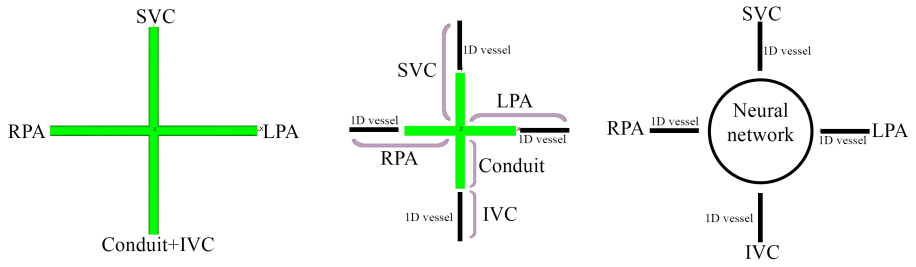

(a) (b) (c)

Figure 3. Computational domains of TCPC for (a) 3D model; (b) 1D–3D multiscale model; (c) 1D-PINN model.

for every first and last node of the grid for the vessel, ψ and ξ depend on the type of approximation. The other boundary conditions commonly state flow and total pressure conservation. See [16, 17] for the detailed definition and other alternatives.

The real TCPC domain is three-dimensional (see Fig. 2a). Integration of a local 3D junction region into a 1D vascular network (see Fig. 2b) is an efficient simplification of the full 3D model. In this work, we establish a relationship between boundary pressures and flows of the 3D TCPC region by the PINN and use the PINN-based mapping (1.3) instead of 3D simulations. For the fixed geometry (i.e., for the given α, β, $\{r_j\}_{j=1}^4$ and dx) we have

$$q_j = F_j(p_1, p_2, p_3, p_4), \quad j = 1, \ldots, 4 \tag{2.5}$$

where j is the index of the appropriate 1D-NN interface (see Fig. 2c), F_j imitates parameters of a 3D flow via the PINN. Thus, for every given set $\{p_j\}_{j=1}^4$ we have a corresponding set $\{q_j\}_{j=1}^4$, which is physically correct in the sense of (1.1).

The iterative numerical algorithm for the coupled 1D–3D simulation (see Fig. 2b) was presented previously in [2]. In this work we use the same methodology for deriving an algorithm for the coupled 1D-NN (see Fig. 2c) simulations.

We assume that numerical solution of the 1D model is known at time t_n. For $n = 0$ the solution is defined by the initial conditions. We set the initial guess for the flows $q_{1D,j}^{(0)}$ at the 1D-PINN interfaces as the linear extrapolation of two previously calculated flows $q_j(t_{n-K})$ and $q_j(t_n)$:

$$q_{1D,j}^{(0)}(t) = q_j(t_{n-K}) + \frac{t - t_{n-K}}{t_n - t_{n-K}} \left(q_j^{(0)}(t_n) - q_j(t_{n-K}) \right), \quad j = 1, \ldots, 4, \quad t_n \leqslant t \leqslant t_{n+K} \tag{2.6}$$

and we run 1D model (2.1) from t_n to t_{n+K} with variable time steps $\tau_k^{(0)}$ ($t_{n+K} - t_n = \sum_{k=1}^K \tau_k^{(0)}$), which are defined by the Courant criterion. For every time step we set the boundary conditions at the 1D-PINN interface as

$$S_j^{(0)}(t)\overline{u}_j^{(0)}(t) = q_{1D,j}^{(0)}(t), \quad j = 1, \ldots, 4, \quad t_n \leqslant t \leqslant t_{n+K}$$

together with the approximation of the compatibility condition along the outgoing characteristic (2.4). For $n = 0$ we assume the flow and total pressure conservation laws similar to the 1D blood flow model

$$\begin{gathered}\sum_{j=1}^{4} q_{1D,j}^{(0)} = 0 \\ \frac{\left(\overline{u}_i^{(0)}\right)^2}{2} + \frac{p_i^{(0)}}{\rho} = \frac{\left(\overline{u}_j^{(0)}\right)^2}{2} + \frac{p_j^{(0)}}{\rho}, \quad i,j = 1,\ldots,4, \;\; i \neq j\end{gathered} \tag{2.7}$$

in the node for the first K time steps to calculate $q_j^{(0)}(t)$, $0 \leqslant t \leqslant t_K$. After that, we update the values

$$\begin{aligned} p_j^{(0)}(t_{n+K}) &= \rho c_{0j}^2 f(S_j^{(0)}(t_{n+K})) \\ q_j^{(0)}(t_{n+K}) &= F_j\left(p_1^{(0)}(t_{n+K}), p_2^{(0)}(t_{n+K}), p_3^{(0)}(t_{n+K}), p_4^{(0)}(t_{n+K})\right), \quad j = 1,\ldots,4 \end{aligned} \tag{2.8}$$

where c_{0j} and S_{0j} are manually defined for vessel j basing on the patient's data, F_j is defined in (2.5).

Finally, we find $p_j(t_{n+K})$, $q_j(t_{n+K})$ at the 1D-PINN interfaces by the following iterative algorithm.

In the present work we set $K = 5 \cdot 10^3$, $\varepsilon = 10^{-9}$, $N_{\max} = 100$, $\chi = 0.09$, $\omega = 0.09$.

3. Results

3.1. Evaluation of PINN training

The dataset used for training the neural networks was generated based on a junction of four vessels with varying angles, radii, and boundary pressures. The length of all segments was set to 7 cm. The radii for the SVC (r_1), LPA (r_2), and RPA (r_4) (see Fig. 2) varied between 0.7 cm and 2.3 cm. The radius of the IVC (r_3) ranged from r_1 to $2.5\,r_1$ for each specific value of r_1. The distance between the centers of the SVC and IVC (dx) was varied from 0 to $r_1 + r_3$ for each combination of r_1 and r_3. Angles between the vessels ranged from 60° to 120°. The boundary pressures were ranged from -100 Pa to 100 Pa.

To systematically explore the multidimensional space of parameters and enhance the diversity of our dataset, we employ the Latin Hypercube Sampling (LHS) method [5]. Let $\mathscr{P}$ represent the parameter space defined by the angles α, β between vessels, the distance dx between the centers of the IVC and SVC, and the radii $\{r_j\}_{j=1}^4$. For each parameter LHS ensures proportional and stratified sampling. The samples are obtained such that the marginal distribution of each parameter is uniformly represented, and correlations between parameters are minimized. Using this approach, we created 100 computational meshes with with various geometric

Algorithm 2.1 Algorithm for computing pressure and flow at the 1D-PINN interfaces

1. Compute the flows at the 1D-PINN interfaces as

$$\widetilde{q}_j^{(i+1)}(t_{n+K}) = (1-\omega)q_{1\mathrm{D,j}}^{(i)}(t_{n+K}) + \omega q_j^{(i)}(t_{n+K}), \quad j = 1,...,4$$

where $q_{1\mathrm{D,j}}^{(i)}(t_{n+K})$ is computed based on the 1D simulations as

$$q_{1\mathrm{D,j}}^{(i)}(t_{n+K}) = S_j^{(i)}(t_{n+K})\overline{u}_j^{(i)}(t_{n+K}). \tag{2.9}$$

2. Run 1D model (2.1) from t_n to t_{n+K} with the updated boundary conditions at the 1D-PINN interfaces

$$S_j^{(i+1)}(t)\overline{u}_j^{(i+1)}(t) = q_j(t_n) + \frac{t-t_n}{t_{n+K}-t_n}\left(\widetilde{q}_j^{(i+1)}(t_{n+K}) - q_j(t_n)\right) \tag{2.10}$$
$$j = 1,\ldots,4, \quad t_n \leqslant t \leqslant t_{n+K}$$

and (2.4). To improve the accuracy of simulations we calculate $S_j^{(i+1)}(t)\overline{u}_j^{(i+1)}(t)$ by the second-order interpolation of $q_j(t_{n+K}), q_j(t_n), q_j(t_{n-K})$.

3. Compute

$$\begin{aligned}
&\widetilde{p}_j^{(i+1)}(t_{n+K}) = \rho c_{0j}^2 f(S_j^{(i+1)}(t_{n+K})) \\
&p_j^{(i+1)}(t_{n+K}) = (1-\chi)p_j^{(i)}(t_{n+K}) + \chi\widetilde{p}_j^{(i+1)}(t_{n+K}) \\
&q_j^{(i+1)}(t_{n+K}) = F_j\left(p_1^{(i+1)}(t_{n+K}), p_2^{(i+1)}(t_{n+K}), p_3^{(i+1)}(t_{n+K}), p_4^{(i+1)}(t_{n+K})\right) \\
&\qquad\qquad j = 1,\ldots,4.
\end{aligned} \tag{2.11}$$

4. Increase i by 1 if $|p^{(i+1)}(t_{n+K}) - p^{(i)}(t_{n+K})| > \varepsilon$ and $i < N_{\max}$ or stop iterations otherwise.

parameters $\{r_j\}_{j=1}^4$, α, β, dx. Next, we apply LHS to generation of 50 inlet and outlet pressure combinations $\{p_j\}_{j=1}^4$ for each mesh resulting in $5 \cdot 10^3$ data samples.

For training the PINN, 80% of the dataset was randomly selected for training, while the remaining 20% was reserved for testing. The technical specifications for the PINN training are: CPU is AMD Ryzen 7 5800X (16) 3.800 GHz, GPU is NVIDIA GeForce GTX 1660 Ti, RAM is 32 GB RAM.

The results indicate that, in both the training and test phases of the study, a convergence trend is evident in the PINN, characterized by decrease in the loss function

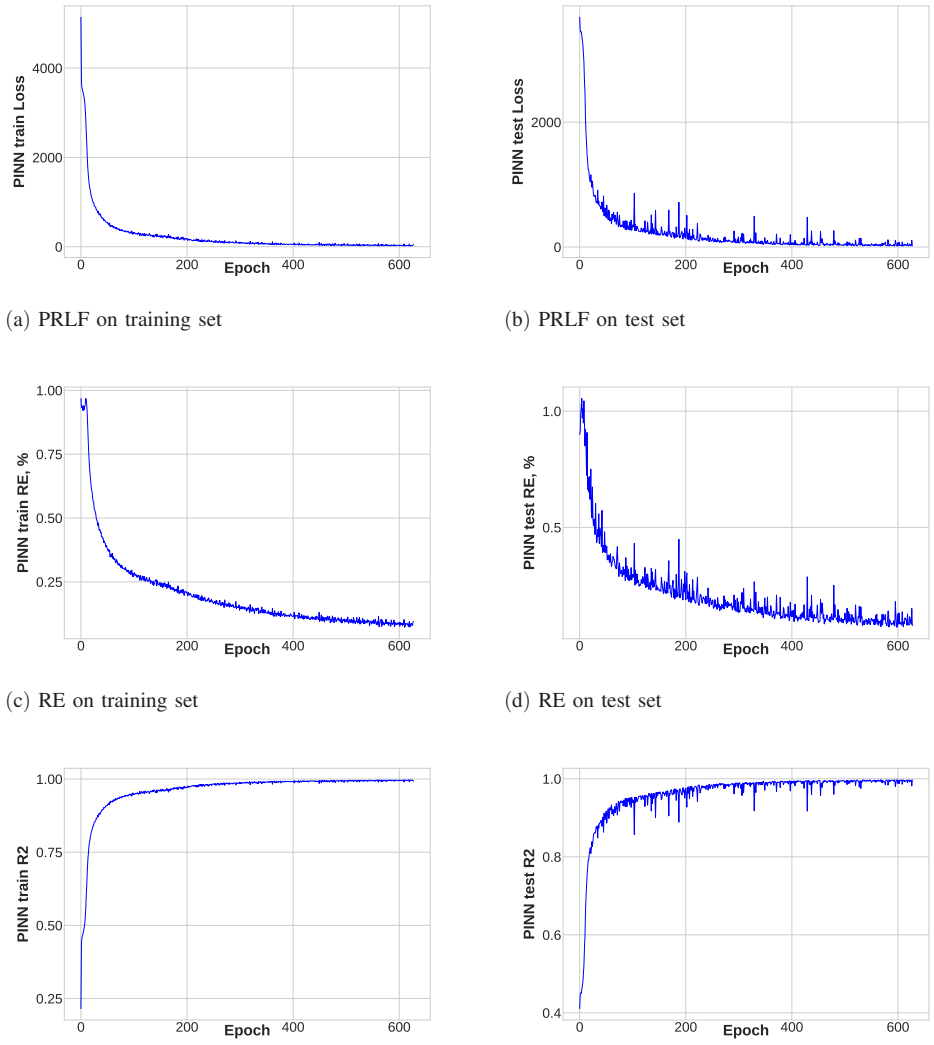

(a) PRLF on training set

(b) PRLF on test set

(c) RE on training set

(d) RE on test set

(e) R2 on training set

(f) R2 on test set

Figure 4. Convergence of the PINN.

in absolute value and the error (RE) function, and increase in the R2 function, which approaches 1 in the limit. The corresponding dependencies are shown in Fig. 4.

Figures 4a and 4b show decrease in absolute loss function (PRLF). The neural network achieves RE values in the range of 6-7% after 600 epochs (see Figs. 4c and 4d), which indicates satisfactory performance. The R2 values shown in Figs. 4e and 4f, indicate that our PINN effectively captures the variation in the targeted variables across both datasets.

Table 1. Geometrical parameters of the computational domains.

Case	Diameter of conduit, cm	α	β	dx, cm
1	1.2	90°	90°	0
2	1.8	90°	90°	0
3	1.2	90°	60°	0
4	1.2	90°	90°	0.6

3.2. Verification of the 1D-PINN network hemodynamic model

In this part we present a set of numerical experiments to simulate blood flow in the TCPC domain. We analyzed the 4D flow MRI mapping data of 8 patients 11–13 years old with Fontan circulation to define the model parameters. The examinations were performed on Siemens 1.5 Tesla Avanto MR tomograph, using a multichannel surface coil for scanning with ECG synchronization. The average diameters of SVC, RPA, and LPA were 1.19 cm, 1.18 cm, and 1.32 cm, respectively. Average forward volume in IVC and SVC was 31.6 ml/s and 11.7 ml/s.

We assume all four vessels (SVC, RPA, LPA and conduit continued by IVC) as straight tubes of length 12 cm with round cross-section. The lengths of conduit and IVC are set to 7 cm and 5 cm, respectively. Diameters of SVC, RPA, LPA, IVC are set to 1.2 cm for all cases. We studied four typical geometries:

Case 1: Four equal mutually perpendicular vessels lie in the same plane (symmetrical cross), diameter of conduit is 1.2 cm (Fig. 5a);

Case 2: The diameter of the conduit is 1.5 times larger than the diameters of the other vessels (Fig. 5b);

Case 3: SVC is at angle 60° to the LPA (Fig. 5c);

Case 4: SVC is shifted 0.6 cm right relative to the conduit (Fig. 5d).

Geometrical parameters of the computational domain are summarized in Table 1.

We set flow rates on the IVC and SVC inflows equal to 31.6 ml/s and 11.7 ml/s based on patient's MRI data analysis. The Poiseuille pressure drop condition is posed as an outflow boundary condition in RPA and LPA: $P = P_{\text{out}} + QR$, where P and Q are pressure and flow rate at the end of the vessel, $P_{\text{out}} = 5$ mmHg is a typical pressure in the healthy heart. Typical pressure for TCPC domain is 14 mmHg. We set the resistance R equal to 553 g/cm^4·s. This value provides the physiologically acceptable pressure drop of 9 mmHg in the case of symmetrical flow distribution between RPA and LPA ($Q = 21.65$ ml/s).

We simulate the blood flow in the considered geometries (see Fig. 5) by three models: 1D-PINN, 1D–3D, and 3D. We compare 1D-PINN results with the results of 1D–3D and 3D simulations in order to validate our new 1D-PINN model.

Figure 3a presents 3D computational domain for the 3D(NS) blood flow model. The model is based on the Navier–Stokes equations. LBB-stable TaylorHood (P2/P1) finite element and backward Euler time stepping are used for the numerical simulations [21]. To cope with convective instabilities in the numerical solution we added

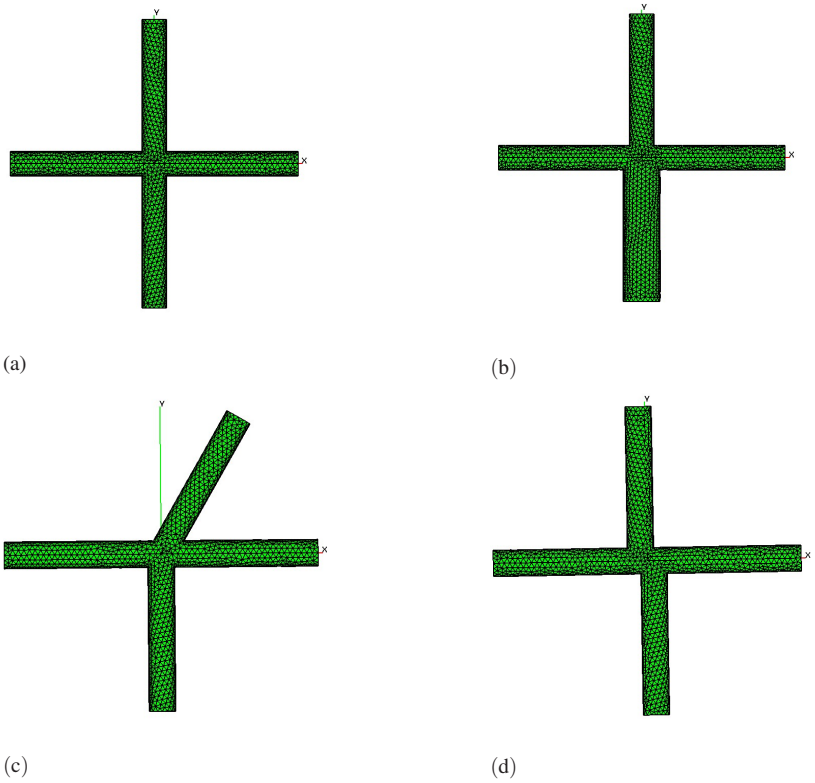

Figure 5. Typical TCPC geometries.

the Smagorinsky turbulence model [13] with weight coefficient 0.2. The flow rates and pressures were averaged over the cross-section and calculated at distance 5 cm from the inflow and the outflow outer boundaries. These cross-sections correspond to the multimodel interfaces in 1D-PINN and 1D–3D models.

The scheme of the computational domain for 1D–3D model is shown in Fig. 3b. The central part of the TCPC domain is considered as a 3D region with rigid walls and the remaining parts of the vessels as 1D regions. The stationary 3D Stokes problem (1.1) is solved at each time step in the 3D domain. Conservation of mass and continuity of pressure are demanded at the interface between 1D and 3D models. Discretization and an algebraic solver of the coupled model are described in [2]. The length of each 1D vessel in both models is set to 5 cm.

The scheme of the computational domain for 1D-PINN model is presented in Fig. 3c. The average number of iterations for the convergence at 1D-PINN interface is from 17 to 26 depending on the geometry.

The results of the simulations include flow rates and pressures at the multimodel interfaces of 1D-PINN and 1D–3D models as well as in the corresponding regions of 3D model. Tables 2 and 3 summarize these values and show the relative difference

Table 2. $q_{SVC}, q_{RPA}, q_{IVC}, q_{LPA}$, calculated by 1D-PINN, 1D–3D and 3D(NS) with the relative difference between 1D-PINN — 1D–3D and 1D-PINN — 3D(NS) models in parentheses.

Case	1D-PINN	1D–3D	3D(NS)
		q_{SVC}, ml/s	
1	11.70	11.70 (0.00%)	11.70 (0.00%)
2	11.70	11.70 (0.00%)	11.70 (0.00%)
3	11.70	11.70 (0.00%)	11.70 (0.00%)
4	11.70	11.70 (0.00%)	11.70 (0.00%)
		q_{RPA}, ml/s	
1	21.37	21.65 (1.29%)	21.65 (1.29%)
2	21.43	21.65 (1.02%)	21.64 (0.97%)
3	21.35	21.65 (1.39%)	21.56 (0.97%)
4	21.40	21.65 (1.15%)	21.80 (1.83%)
		q_{IVC}, ml/s	
1	31.60	31.60 (0.00%)	31.60 (0.00%)
2	31.60	31.60 (0.00%)	31.60 (0.00%)
3	31.60	31.60 (0.00%)	31.60 (0.00%)
4	31.60	31.60 (0.00%)	31.60 (0.00%)
		q_{LPA}, ml/s	
1	21.40	21.65 (1.15%)	21.63 (1.06%)
2	21.44	21.65 (0.97%)	21.65 (0.97%)
3	21.40	21.65 (1.15%)	21.71 (1.43%)
4	21.44	21.65 (0.97%)	21.50 (0.28%)

between 1D-PINN and 1D–3D as well as between 1D-PINN and 3D(NS) for the sake of comparison.

From Tables 2 and 3 we can conclude that the 1D-PINN model shows little relative difference from the 1D–3D model. The maximum deviation, both in terms of pressure and flow rate, does not exceed 1.48%. Since the same 3D model was used both for the 3D part in the 1D–3D model and for the PINN training, this observation reconfirms the successful performance of the PINN (rf. to Section 3.1). There is a slight asymmetry in the flow distribution between RPA and LPA and a loss of fluid within 1–1.3% in the 1D-PINN model. Most likely the PINN systematically underestimates pressure by 0.6–1.5%.

The 3D(NS) model provides the pressure drop between the inflow and outflow boundaries of the central TCPC region in the range of 0.8–1.65 mmHg. It is much greater than the pressure drop in the 1D-PINN and 1D–3D models (0.11–0.22 mmHg). The difference in pressure between the models can be attributed to the fact that the 3D(NS) model incorporates inertial forces resulting from the convective term. Maximum relative difference between the pressures calculated by the 1D-PINN and 3D(NS) models is 12.26%.

Basing on the 3D(NS) simulations we observe the difference in hemodynamic parameters depending on the geometrical configuration. Increasing the diameter of the conduit leads to a general decrease in TCPC pressure: in Case 2 the pressure in vena cava is lower by 0.66 mmHg. Changing the connection angle of the SVC or shifting the SVC relative to the IVC leads to the blood redistribution between RPA and LPA: 49.83% of blood goes to RPA in Case 3 and 50.35% in Case 4. The central pressure decreases as well but less significantly than in Case 2. At the same time the

Case	1D-PINN	1D–3D	3D(NS)
		p_{SVC}, mmHg	
1	13.96	14.11 (1.06%)	15.91 (12.26%)
2	13.99	14.11 (0.85%)	15.24 (8.20%)
3	13.96	14.11 (1.06%)	15.82 (11.76%)
4	13.97	14.11 (0.99%)	15.60 (10.45%)
		p_{RPA}, mmHg	
1	13.85	13.97 (0.86%)	14.26 (2.88%)
2	13.88	13.97 (0.64%)	14.26 (2.66%)
3	13.85	13.97 (0.86%)	14.22 (2.60%)
4	13.87	13.97 (0.72%)	14.31 (3.07%)
		p_{IVC}, mmHg	
1	13.98	14.19 (1.48%)	15.72 (11.07%)
2	13.98	14.08 (0.71%)	15.06 (7.17%)
3	13.98	14.19 (1.48%)	15.68 (10.84%)
4	14.00	14.19 (1.34%)	15.56 (10.03%)
		p_{LPA}, mmHg	
1	13.87	13.97 (0.72%)	14.26 (2.73%)
2	13.88	13.97 (0.64%)	14.25 (2.60%)
3	13.87	13.97 (0.72%)	14.29 (2.94%)
4	13.88	13.97 (0.64%)	14.19 (2.18%)

Table 3. $p_{\mathrm{SVC}}, p_{\mathrm{RPA}}, p_{\mathrm{IVC}}, p_{\mathrm{LPA}}$, calculated by 1D-PINN, 1D–3D and 3D(NS) with the relative difference between 1D-PINN — 1D–3D and 1D-PINN — 3D(NS) models in parentheses.

maximal relative deviation between the flow rates calculated by the 1D-PINN and full 3D models is 1.83%.

4. Conclusions

This paper presents new junction conditions for one-dimensional network hemodynamic model for the total cavopulmonary connection generated by the Fontan operation. The conditions include physically informed neural network trained with 3D stationary Stokes flow model, satisfying mass conservation constraint. We extend the combination of 1D and 3D models developed earlier to the combination of 1D and PINN models which is less expensive computationally. The novel junction conditions of the 1D network model account for the geometric parameters of the complex vascular junction, including such aspects as angles between the four vessels and their respective shift. Clearly, the methodology described here can be applied in a similar manner to the analysis of vascular junctions exhibiting alternative anatomic and surgically induced geometries. To the best of our knowledge, no other works have been identified that exhibit comparable functionality. Nevertheless, the present result represents the initial phase in the development of a PINN-based boundary conditions for complex vascular junctions in a 1D network model, which are based on 3D dynamic Navier–Stokes simulations with elastic moving walls.

The results show decrease of the PINN's error function to the tolerance of 7% after 600 epochs of training. There is acceptable variation in both training and test data sets. The 1D-PINN model shows good agreement with the reference 1D-3D

model in four typical geometries. It can be stated that the maximum deviations of averaged pressures and flows do not exceed 1.48%. The 1D-PINN model demonstrates a satisfactory degree of agreement with the dynamic 3D Navier–Stokes model, exhibiting maximum deviation of 12.26%.

In this study, a steady-flow model ignoring inertia forces is utilised for the purposes of PINN training. Therefore, the distinction between 1D-PINN and 3D(NS) is considerable. These deficiencies will be rectified in the subsequent phase of research. In this regard, the forthcoming work will entail the implementation of the Navier–Stokes model as the underlying foundation for PINN training. Furthermore, additional testing and validation of the model are necessary, employing a greater number of geometric models and real patient data, in order to enhance its reliability.

The 3D Navier–Stokes model is regarded as a benchmark for its capacity to provide a more accurate representation of fluid flow dynamics by incorporating the convective term and time. In the future research, we shall use 3D fluid–structure interaction simulation as a point of reference as the most physiologically appropriate model of flows in TCPC.

The proposed approach permits the incorporation of locally complex flow patterns into extended one–dimensional network hemodynamic model at the relatively low computational cost and with notable efficiency. By employing this methodology, one can assess the geometric properties of the vessel junction region, which is a distinctive attribute absent in the majority of contemporary 1D models. The potential of the proposed methodology has been illustrated through the analysis of representative instances of vessel anastomosis generated by the Fontan procedure.

References

1. P. R. Amestoy, I. S. Duff, J.-Y. L'Excellent, and J. Koster, A fully asynchronous multifrontal solver using distributed dynamic scheduling. *SIAM Journal on Matrix Analysis and Applications* **23** (2001), No. 1, 15–41.

2. T. Dobroserdova, M. Olshanskii, and S. Simakov, Multiscale coupling of compliant and rigid walls blood flow models. *Int. J. Numer. Meth. Fluids* **8** (2016), 799–817.

3. M. Du, C. Zhang, S. Xie, F. Pu, D. Zhang, and D. Li, Investigation on aortic hemodynamics based on physics-informed neural network. *Mathematical Biosciences and Engineering* **20** (2023), 11545–11567.

4. C. Geuzain and J. Remacle, Gmsh: A 3-d finite element mesh generator with built-in pre- and post-processing facilities. *International Journal for Numerical Methods in Engineering* **79** (2009), 1309–1331.

5. J. Helton and F. Davis, Latin hypercube sampling and the propagation of uncertainty in analyses of complex systems. *Reliability Engineering and System Safety* **81** (2003), No. 1, 23–69.

6. A. Isaev, T. Dobroserdova, A. Danilov, and S. Simakov, Physically informed deep learning technique for estimating blood flow parameters in four-vessel junction after the Fontan procedure. *Computation* **12** (2024), 41.

7. D. Kingma, Adam: A method for stochastic optimization. *arXiv:1412.6980*, 2014.

8. A. Krizhevsky, I. Sutskever, and G. Hinton, Imagenet classification with deep convolutional neural networks. *Communications of the ACM* **60** (2012) 84–90.

9. J. Kutz, Deep learning in fluid dynamics. *Journal of Fluid Mechanics* **814** (2017), 1–4.

10. K. Magomedov and A. Kholodov, *Grid-Characteristics Numerical Methods*, 2nd ed. Urait, Moscow, 2018.

11. M. A. Nabian and H. Meidani, Physics–informed regularization of deep neural networks. *arXiv:1810.05547*, 2018.

12. R. Rojas, *The Backpropagation Algorithm*. Springer, Berlin–Heidelberg, 1996, Ch. 7, pp. 149–182.

13. P. Sagaut, *Large Eddy Simulation for Incompressible Flows: An Introduction*. Springer Science & Business Media, 2006.

14. M. Sarabian, H. Babaee, and K. Laksari, Physics-informed neural networks for brain hemodynamic predictions using medical imaging. *IEEE Transactions on Medical Imaging* **41** (2022), No. 9, 2285–2303.

15. D. Siallagan, Y.-H. Loke, L. Olivieri, J. Opfermann, C. Ong, D. De Zélicourt, A. Petrou, M. Daners, V. Kurtcuoglu, M. Meboldt, K. Nelson, L. Vricella, J. Johnson, N. Hibino, and A. Krieger, Virtual surgical planning, flow simulation, and 3-dimensional electrospinning of patient-specific grafts to optimize Fontan hemodynamics. *Journal of Thoracic and Cardiovascular Surgery* **155** (2018), No. 4, 1734–1742.

16. S. Simakov, Modern methods of mathematical modeling of blood flow using reduced order methods. *Computer Research and Modeling* **5** (2018), 581–604.

17. S. Simakov, New boundary conditions for one-dimensional network models of hemodynamics. *Computational Mathematics and Mathematical Physics* **61** (2021), 2102–2117.

18. N. Srivastava, G. Hinton, A. Krizhevsky, I. Sutskever, and R. Salakhutdinov, Dropout: A simple way to prevent neural networks from overfitting. *Journal of Machine Learning Research* **15** (2014), 1929–1958.

19. Y. Vassilevski and K. Lipnikov, An adaptive algorithm for quasioptimal mesh generation. *Comp. Math. Math. Phys.* **39** (1999), 1468–1486.

20. Y. Vassilevski, V. Salamatova, and S. Simakov, On the elasticity of blood vessels in one-dimensional problems of hemodynamics. *Comput. Math. and Math. Phys.* **55** (2015), 1567–1578.

21. Y. Vassilevski, M. Olshanskii, S. Simakov, A. Kolobov, and A. Danilov, *Personalized Computational Hemodynamics*. Elsevier, 2020.

22. W. Yang, F. Chan, V. Reddy, A. Marsden, and J. Feinstein, Flow simulations and validation for the first cohort of patients undergoing the y-graft Fontan procedure. *The Journal of Thoracic and Cardiovascular Surgery* **149** (2015), 247–255.

23. D. de Zélicourt and V. Kurtcuoglu, Patient-specific surgical planning, where do we stand? The example of the Fontan procedure. *Annals of Biomedical Engineering* **44** (2015), 174–186.